Optics Communications 283 (2010) 1917–1923

Contents lists available at ScienceDirect

Optics Communications

journal homepage: www.elsevier.com/locate/optcom

Four Wave Mixing spectroscopy at the interface between the time and frequency domains

Yuri Paskover [1], Andrey Shalit [*,1], Yehiam Prior

Department of Chemical Physics, Weizmann Institute of Science, Rehovot 76100, Israel

ARTICLE INFO

Article history:
Received 19 October 2009
Received in revised form 30 December 2009
Accepted 30 December 2009

Keywords:
Four wave mixing
Phase matching
Time resolved spectroscopy

ABSTRACT

We demonstrate a new approach to Four Wave Mixing spectroscopy involving simultaneous measurements at time and frequency domains, where spectral selectivity is achieved by phase matching filtering, and the time resolution is obtained within a single ultra-short pulse. We analyze the Four Wave Mixing signal, and show that our method is capable for discrimination between different spectroscopic pathways of vibrational coherences modulating the scattered signal.

1. Introduction

Spectrally and temporally resolved measurements are considered to be complementary, and the choice of one or the other is usually based on practical considerations such as the signal to noise ratio of a specific experiment. Coherent spectroscopy with ultra-short pulses enables direct observation of specific transitions, as well as real time tracking of intramolecular pathways of coherence or energy redistribution. The inherently broad bandwidth of ultra-short pulses provides an opportunity for simultaneous excitation of multiple degrees of freedom and for measurement of their interactions [1], as in multidimensional NMR [2,3].

In a typical time resolved Four Wave Mixing (FWM) experiment, the molecular dynamics is being probed by three laser pulses, where the first two are used to excite a vibrational/rotational wavepacket via a stimulated Raman type process, and a third, time delayed pulse, stimulates coherent emission of the FWM signal in the phase matching direction [4]. With the extremely broad bandwidth of ultra-short pulses, the classification of such experiments to CARS (Coherent Anti-Stokes Raman Scattering), CSRS (Coherent Stokes Raman Scattering) or DFWM (Degenerate Four Wave Mixing) might be misleading and therefore we will use the generic term Four Wave Mixing. Combined time and frequency domain measurements of coherent molecular dynamics were demonstrated to simplify the interpretation of the retrieved data. Heid et al. [5] reported on spectrally dispersed femtosecond time-resolved CARS for the investigation of the electronic ground-state vibrational dynamics of complex molecules in solution. They showed that the two-dimensional mapping allows for interpretation of the complex signal produced by molecules with a large number of molecular vibrations. Prince et al. [6] suggested a variant of time-resolved CARS that allows for multiplex detection of Raman active modes on the ground and excited electronic states. More recently, Nath et al. [7,8] showed that for CARS, simultaneous detection in the time and frequency domains provides information even when the pulse durations and spectral widths do not allow either full temporal or full spectral resolution. Moreover, these authors have shown that from the combined Time-Frequency Domain (TFD) measurements one can derive the full (amplitude and phase) information for the third order susceptibility $\chi(3)$. Similar results were recently demonstrated by Konorov et al. [9] and Xu et al. [10] who have shown that an arrangement similar to XFROG [11] is useful for the full characterization of the third order susceptibility from TFD data.

In this work we demonstrate how the full TFD information can be derived with only a small number of laser pulses. We show that measurements in the TFD domain facilitate the deciphering of the observed temporal dynamics, and enable us to fully identify fundamental and beat modes observed in the spectrum.

The structure of the paper is as follows: we first discuss 'standard' TFD measurement of chloroform where the probe delay is mechanically scanned, and for each delay the full spectrum of the signal is measured. We provide a detailed analysis of the coherent pathways (Feynman diagrams) leading to the generation of the signal, and show how the TFD information is useful for the characterization of the observed data. Next we introduce a new very

* Corresponding author.
E-mail address: andrey.shalit@weizmann.ac.il (A. Shalit).
[1] These authors made an equal contribution to this work.

0030-4018/$ - see front matter © 2010 Elsevier B.V. All rights reserved.
doi:10.1016/j.optcom.2009.12.078

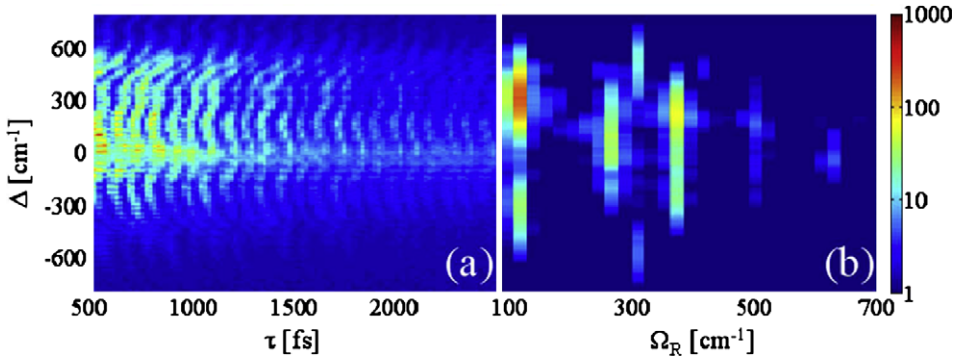

Fig. 1. (a) Spectrally and temporally resolved FWM signal from neat chloroform ($CHCl_3$). (b) Horizontal line by line Fourier Transform of part (a) depicting the power spectrum at each Raman frequency (the intensity is given on log scale). Δ is detuning from the laser center frequency in cm^{-1}.

rapid approach to the observation of the TFD. The new method is a combination of our previously demonstrated single-shot CARS measurement [12] and a newly introduced Phase Matched Filtering (PMF). We conclude the paper with a discussion of the advantages and limitations of this new approach.

2. Combined time frequency measurements

Consider a time resolved FWM experiment in the now standard three-dimensional folded boxcars phase matching geometry [13], carried out on neat liquid chloroform. The three input pulses (pump, dump and probe) are derived from the same regeneratively amplified laser (60 fs, 800 nm central frequency, ~1 mJ per pulse, 1 kHz repetition rate). The generated FWM signal is spectrally dispersed in a spectrometer before being detected on a CCD. The first two pulses create a ground state coherent superposition of vibrational states, which scatters a time delayed probe pulse, generating the FWM signal. Fig. 1a depicts a spectrogram of such measurements: for each delay of the probe pulse (horizontal axis) the FWM signal is spectrally resolved on the spectrometer (vertical axis). In this spectrogram, the vertical axis is calibrated in terms of the frequency detuning of the detected signal from the laser center frequency (around 800 nm). The horizontal axis is the probe delay mechanically scanned over the range of 500–2500 fs with a 20 fs step size. The measurement was intentionally started at $\tau = 500$ fs to avoid the very strong coherence peak.

Fig. 1b is a composite horizontal line by line Fourier Transform of the data in Fig. 1a. Thus, the horizontal axis is now converted to the frequency domain, showing the spectral contents (vertical axis) of the generated FWM signal at each frequency (horizontal axis). In Fig. 1b, several prominent features are observed around 104, 261, 300, 365 and 625 cm^{-1}. These are fundamental vibrational modes as well as beat frequencies between them. There is an additional feature around 500 cm^{-1}, which may originate from higher modes, but is not fully analyzed at this point. As noted above, these measurements of low frequency Raman modes are similar and complementary to the measurements by Nath et al. [8] and Urbanek et al. [14].

Fig. 1b reveals differences between the detuning dependence of signals at different Raman frequencies. As an example, the signal at 625 cm^{-1} is centered around zero detuning from the laser frequency, while the signal at 104 cm^{-1} appears to be split, peaking around ±310 cm^{-1}. This additional information, not available in either the time or frequency domains alone, is useful for the characterization of the observed modes, as is discussed theoretically in the next section. However, already at this point it should be noted that the acquisition of a signal of the type depicted in Fig. 1 takes a long time, as the delay needs to be scanned mechanically, and for each delay, the spectrum is acquired with proper signal averaging. Long measurement times may pose a problem for molecules which are not stable against photobleaching, and in particular in cases of resonant excitation. Thus, a significant advantage will be added when the full signal can be captured on a much faster time scale, as is discussed below.

3. Theoretical background

In this section we consider Time Resolved FWM (TRFWM) in which all input pulses are derived from the same ultra-short laser and have the same spectral properties. All Raman type two photon transitions are derived from the spectral components included within the bandwidth of the pulses. The observed signal is produced when the probe pulse is scattered by the third order polarization induced in the medium by the first two pulses.

Perturbation theory provides a formal description for this nonlinear polarization:

$$P^{(3)}(t) = \left\langle \Psi^{(0)}(t)\left|\hat{\mu}\right|\Psi^{(3)}(t)\right\rangle + \left\langle \Psi^{(1)}(t)\left|\hat{\mu}\right|\Psi^{(2)}(t)\right\rangle + c.c. \quad (1)$$

Here $P^{(3)}(t)$ is the third order polarization, $\Psi^{(n)}(t)$ is wavefunction representing the state of the molecule after interaction with n fields, and $\hat{\mu}$ is the transition dipole operator (assumed, for simplicity, to be the same for all transitions).

As is well established, there are many coherent pathways leading to the third order susceptibility, involving the same input frequencies, but differing in their time ordering. These pathways are

Table 1
The two leading processes contributing to the third order polarization in non-resonant time delayed FWM in 3D folded boxcars configuration. The left column depicts the double-sided Feynman diagrams while the right column sketches the corresponding energy level diagram. The solid and dashed lines symbolize the "ket" and the "bra" side transitions, respectively.

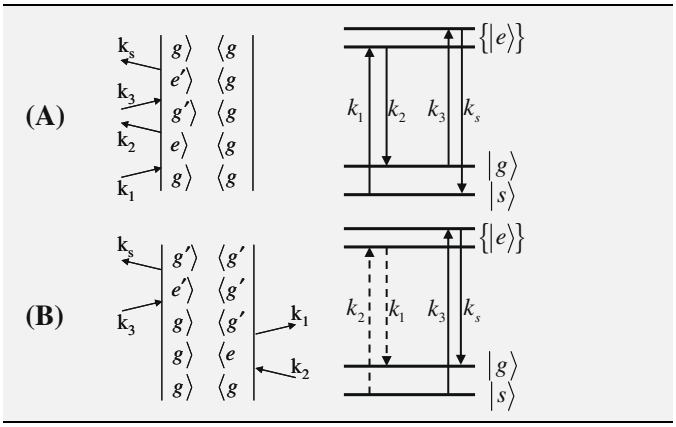

conveniently represented by double-sided Feynman diagrams [15]. For the configuration of a non-resonant TRFWM in a three-dimensional boxcars configuration, there are two dominant diagrams, which are given in Table 1 (we have verified that the non-RWA terms do not have a significant effect on the final result).

For this theoretical consideration, and for simplicity, the input laser fields are assumed to be transform limited pulses described by:

$$E_n(t) = \varepsilon_n(t)e^{-i\omega_n t} + c.c. = \frac{1}{\sqrt{2\pi}}\int_{-\infty}^{\infty} d\omega S_n(\omega)e^{-i\omega t} + c.c.$$

Here $E_n(t)$ is the electric field of the pulse, $\varepsilon_n(t)$ is the pulse envelope, ω_n is its carrier frequency, $S_n(\omega)$ is the spectral amplitude of the nth pulse (here the same for all pulses).

To lowest order of perturbation the expressions for the third order polarization for each of the diagrams (A,B) are given by:

$$P_A^{(3)}(t,\tau) = i\sum_g \frac{|\langle s|\hat{\alpha}_g|g\rangle|^2}{2\pi\Delta^2\hbar^3}\varepsilon_3(t)e^{-i[(\omega_3+\Omega_g)t+\Omega_g\tau]}R_{1,2}(\Omega_g) + c.c., \quad (2)$$

$$P_B^{(3)}(t,\tau) = -i\sum_g \frac{|\langle s|\hat{\alpha}_g|g\rangle|^2}{2\pi\Delta^2\hbar^3}\varepsilon_3(t)e^{-i[(\omega_3-\Omega_g)t-\Omega_g\tau]}R_{2,1}^*(\Omega_g) + c.c. \quad (3)$$

Here τ represents the probe delay, Δ is the nominal detuning of the laser frequency from the nearest electronic transition, the index g accounts for all allowed vibrational transitions, each with frequency Ω_g and polarizability $\hat{\alpha}_g$. Note, that for a set of input pulses, the bandwidth available for excitation at of frequency Ω is given by a combination of the frequency components derived from the input pulses:

$$R_{m,n}(\Omega) = \int_{-\infty}^{\infty} d\omega S_m(\omega)S_n^*(\omega-\Omega).$$

In a recent paper [16] we have analyzed in detail the generation of a Time Resolved Four Wave Mixing signal, and have shown that unless the FWM signal is linearized, only combination frequencies are observed and the fundamental vibrational frequencies are not present in the signal. We have further shown that the presence of slow rotational excitation in the system gives rise to in-situ heterodyne detection, thus linearizing the signal. When a slow rotational contribution is added, the total polarization of the medium can be written as

$$P_{Tot}^{(3)}(t,\tau) = P_{rot}^{(3)}(t) + \sum_g [P_A^{(3)}(t,\Omega_g,\tau) + P_B^{(3)}(t,\Omega_g,\tau)].$$

Because of its slow response, the rotational polarization is independent of the probe delay. The spectral properties of the field produced by each one of the components of the polarization may be obtained by its direct transform from the time to the frequency domain.

$$\begin{aligned} P_{rot}^{(3)}(\omega) &\propto S_3(\omega) \\ P_A^{(3)}(\omega,\Omega_g,\tau) &\propto S_3(\omega-\Omega_g)e^{-i\Omega_g\tau} + c.c. \\ P_B^{(3)}(\omega,\Omega_g,\tau) &\propto S_3(\omega+\Omega_g)e^{i\Omega_g\tau} + c.c. \end{aligned} \quad (4)$$

The detected quantity is the intensity of the emitted signal, and thus proportional to the modulus square of the total polarization.

$$\begin{aligned} I(\omega,\tau) &\propto |P_{Tot}^{(3)}(\omega,\tau)|^2 \\ &= |P_{rot}^{(3)}(\omega,\tau)|^2 + \sum_{g,g'}\{P_A^{(3)}(\omega,\Omega_g,\tau)[P_A^{(3)}(\omega,\Omega_{g'},\tau)]^* \\ &\quad + P_B^{(3)}(\omega,\Omega_g,\tau)[P_B^{(3)}(\omega,\Omega_{g'},\tau)]^*\} + \sum_g\{P_A^{(3)}(\omega,\Omega_g,\tau) \\ &\quad \times [P_{rot}^{(3)}(\omega,\tau)]^* + P_B^{(3)}(\omega,\Omega_g,\tau)[P_{rot}^{(3)}(\omega,\tau)]^*\} \\ &\quad + \sum_{g,g'}\{P_A^{(3)}(\omega,\Omega_g,\tau)[P_B^{(3)}(\omega,\Omega_{g'},\tau)]^* + P_B^{(3)}(\omega,\Omega_g,\tau) \\ &\quad \times [P_A^{(3)}(\omega,\Omega_{g'},\tau)]^*\} + c.c. \end{aligned} \quad (5)$$

The first term in Eq. (5), as well as those cases of the second term where $g = g'$ do not show any intensity oscillations as a function of probe delay.

The second term of Eq. (5) contains terms where $g \neq g'$. Such terms then take a form:

$$\begin{aligned} I_2(\omega,\tau) &\propto \sum_{g\neq g'}\{S_3(\omega-\Omega_g)S_3^*(\omega-\Omega_{g'})e^{-i[\Omega_g-\Omega_{g'}]\tau} \\ &\quad + S_3(\omega+\Omega_g)S_3^*(\omega+\Omega_{g'})e^{i[\Omega_g-\Omega_{g'}]\tau}\} + c.c. \end{aligned}$$

This expression shows oscillations at $(\Omega_g - \Omega_{g'})$, the difference between vibrational modes, and the amplitude of the oscillations depends on the optical detection frequency ω.

For a pair of states with energies Ω_g and $\Omega_{g'}$ this combination frequency oscillation will have its maximal amplitude at the maximum of spectral overlap of the two fields: $S_3(\omega-\Omega_g)S_3^*(\omega-\Omega_{g'})$ and $S_3(\omega+\Omega_g)S_3^*(\omega+\Omega_{g'})$. For pulses of a symmetric Gaussian spectrum, these maxima occur at $\omega = \omega_3 \pm \frac{\Omega_g+\Omega_{g'}}{2}$.

The third term in Eq. (5) is a result of interference between vibrational and "slow" rotational contributions to the nonlinear polarization, and therefore shows intensity oscillations at the fundamental molecular vibrational frequencies:

$$\begin{aligned} I_3(\omega,\tau) &\propto \sum_g\{S_3(\omega-\Omega_g)S_3^*(\omega)e^{-i\Omega_g\tau} + S_3(\omega+\Omega_g)S_3^*(\omega)e^{i\Omega_g\tau}\} \\ &\quad + c.c. \end{aligned}$$

Along the lines of the previous analysis, the amplitude of the intensity oscillations at Ω_g would be maximized at $\omega = \omega_3 \pm \frac{\Omega_g}{2}$, the best spectral overlap between the two contributions.

The fourth term of Eq. (5) indicates interference between two different coherence pathways. Since the contributions of these coherence pathways are symmetric around the carrier frequency, the spectral overlap is maximized around zero detuning. In addition, the interference of the two pathways gives rise to sums of fundamental frequencies, including doubled fundamental frequencies.

$$\begin{aligned} I_4(\omega,\tau) &\propto \sum_{g\neq g'}\{S_3(\omega-\Omega_g)S_3^*(\omega+\Omega_{g'})e^{-i[\Omega_g+\Omega_g']\tau} \\ &\quad + S_3(\omega+\Omega_g)S_3^*(\omega-\Omega_{g'})e^{i[\Omega_g+\Omega_{g'}]\tau}\} + c.c. \end{aligned}$$

To summarize this brief theoretical analysis, in TRFWM in the degenerate case one expects to find the following:

1. Oscillations at the fundamental mode frequencies are most observable at detection frequency detuned (to the blue or to the red) from the carrier by half of a vibrational quantum.
2. Oscillations at difference of fundamental vibrational modes frequencies are maximal at detection frequency that is detuned from the carrier by the average of the fundamental modes.
3. Oscillations at sums and doubles of the fundamental vibrational frequencies are maximal at the vicinity of zero detuning from the carrier frequency.

4. Phase matching filtering (PMF)

The measurement of a full spectrogram requires a long time, which may be a problem for some molecules. We now present a way to obtain the two-dimensional spectrally resolved information rapidly and without mechanical scanning of delay lines.

We use the forward propagating three-dimensional (boxcars) geometry [13,17] where the three input beams constitute the three edges of a square pyramid, and the generated signal completes the fourth edge on the other side of the interaction region (Fig. 2a).

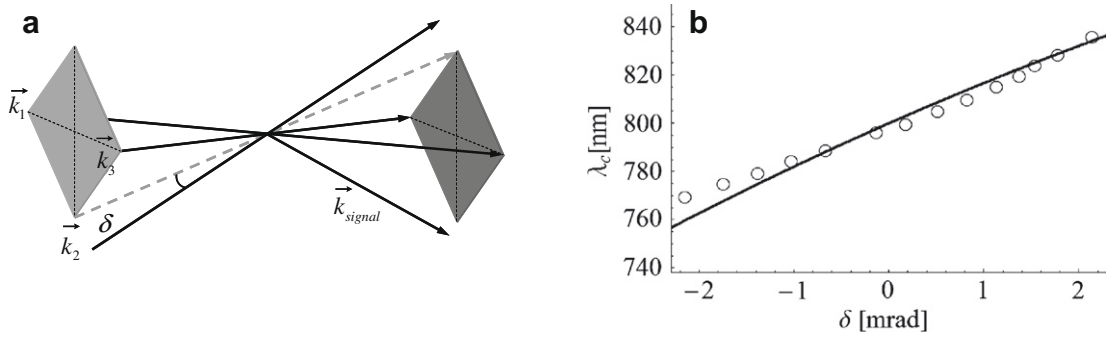

Fig. 2. (a) The 3D-boxcars configuration, with the Stokes beam deviation angle δ. (b) Central frequency of phase matching filtered FWM signal as function of δ measured (open circles) and calculated (line).

Recently we have reported the use of collimated (unfocused) beams in this FWM arrangement for single shot time resolved measurements [12], where the different arrival times of the pulses to different points in the beams' intersection region map the time delays between the pulses. Direct imaging of the signal emerging from each point in the intersection resulted in a picture of several picoseconds of vibrational motion captured by a single ultra-short laser pulse. By tuning the angle of one of the beams away from a symmetric square pyramid we are able to tune the FWM phase matching frequency, thus tuning the observed generated frequency within the wide spectrum available from the ultra-short pulses. The implemented technique is conceptually akin to the well known pulse characterization method of GRENOUILLE [18], that employs strict phase matching for spectral resolution of nonlinear signals.

The coherent generation of a FWM signal fulfills two criteria: conservation of energy

$$\omega_s = \omega_1 - \omega_2 + \omega_3, \tag{6}$$

and conservation of momentum or phase matching:

$$[\omega_1 \hat{k}_1 n(\omega_1) - \omega_2 \hat{k}_2 n(\omega_2) + \omega_3 \hat{k}_3 n(\omega_3)]/c = \omega_s \hat{k}_s n(\omega_s)/c. \tag{7}$$

Here ω_i, and $\hat{k}_i$ represent the frequency and direction of propagation for each of the beams and $n(\omega)$ is the refractive index of the medium. For transparent media one may assume for simplicity a refractive index that is constant over the entire relevant spectral range.

Traditionally the beams are focused into the interaction region, such that each beam contains a range of propagation directions. This virtually relaxes the phase matching constraints such that all energetically allowed combinations of frequency components contribute to the signal. Assuming a Gaussian spectral shape for the incident pulses of the form: $S(\omega) = \varepsilon e^{-\frac{(\omega-\omega_0)^2}{\sigma^2}}$ we obtain the spectral contents of the generated signal in the case of focused beams:

$$\begin{aligned} E_s(\omega_s) &= \int_{-\infty}^{\infty}\int_{-\infty}^{\infty} d\omega_1 d\Omega S(\omega_1) S^*(\omega_2 = \omega_1 - \Omega) S(\omega_3 = \omega_s - \Omega) \\ &= \frac{\pi\varepsilon^3\sigma^2}{\sqrt{3}} e^{\frac{(\omega_s-\omega_0)^2}{(\sigma\sqrt{3})^2}}. \end{aligned} \tag{8}$$

Here $E_s(\omega_s)$ is the amplitude of the generated field at a frequency ω_s, ε the amplitude of the laser pulse, σ is the pulse's bandwidth and ω_0 is its carrier frequency. Because various input frequencies combine to generate the nonlinear signal, the bandwidth of the generated signal is larger (by a factor of $\sqrt{3}$) than that of the input pulses.

The geometrical arrangement of our experiment (Fig. 2a) involves unfocused, collimated beams for which the propagation direction is very well defined [12]. The intersection of the collimated beams is spatially long (several cm), and thus it defines strict phase matching constrains on the interaction between the spectral components of the pulses (for recent detailed discussions of this subject, see Romanov et al. [19], Belabes et al. [20] and Naumov et al. [21]). We use this Phase Matching Filtering for spectrally resolving the FWM signal.

Fig. 2a sketches the 3D folded boxcars geometry where the propagation of the Stokes ($\mathbf{k}_2$) beam is detuned by an angle δ from the symmetric (square) configuration.

The unit propagation vectors of each one of the beams are defined as follows:

$$\vec{k}_1 = \begin{pmatrix} \cos\theta \\ \sin\theta \\ 0 \end{pmatrix}; \quad \vec{k}_2 = \begin{pmatrix} \cos\varphi \\ 0 \\ \sin\varphi \end{pmatrix}; \quad \vec{k}_3 = \begin{pmatrix} \cos\theta \\ -\sin\theta \\ 0 \end{pmatrix}. \tag{9}$$

where 2θ is the angle between pump and probe beams ($\mathbf{k}_1$ and $\mathbf{k}_3$), and $\varphi = \theta + \delta$.

For convenience, define Ω and ζ:

$$\begin{aligned} \Omega &\equiv \omega_1 - \omega_2 \\ \zeta &\equiv \omega_s - \omega_1 \end{aligned} \tag{10}$$

Using Eq. (6) $\omega_3 = \omega_s - \Omega$.

Substituting Eq. (10) into Eq. (7) we obtain an equation for ζ:

$$[\omega_s - \zeta]\hat{k}_1 - [\omega_s - \zeta - \Omega]\hat{k}_2 + [\omega_s - \Omega]\hat{k}_3 = \omega_s \hat{k}_s. \tag{11}$$

For pulses which are not "too short" ($\sigma \ll \omega_0$) we use the relation $\Omega \ll \omega_s$ and expand in a power series of Ω. To first order we derive a solution for ζ

$$\zeta = a(\theta,\delta)\Omega + b(\theta,\delta)\omega_s. \tag{12}$$

where the coefficients $a(\theta,\delta)$ and $b(\theta,\delta)$ depend only on the geometry of the experiment.

$$\begin{aligned} a &= -\frac{\cos\delta - 2\cos(2\theta) + \cos(2\theta+\delta)}{-2 + \cos\delta + \cos(2\theta+\delta)} - \frac{4\sin^2\theta}{\cos\delta - 2\cos(2\theta) + \cos(2\theta+\delta)}; \\ b &= \frac{4\cos\theta(\cos(\theta+\delta) - \cos\theta)}{-2 + \cos\delta + \cos(2\theta+\delta)}. \end{aligned} \tag{13}$$

By superposing all the allowed combinations of spectral components of the input pulses we calculate $E_{PM}(\omega_s;\theta,\delta)$ which is the phase-matched FWM signal field amplitude for a particular choice of angels between the incident beams:

$$E_{PM}(\omega_s;\theta,\delta) = \int_{-\infty}^{\infty} d\Omega S(\omega_s - \zeta) S^*(\omega_s - \zeta - \Omega) S(\omega_s - \Omega). \tag{14}$$

For the same Gaussian input pulses the phase-matched FWM spectrum may be represented as:

$$E_{PM}(\omega_s;\theta,\delta) \propto e^{-\frac{4\ln 2(\omega_s-\omega_c)^2}{(\Delta\omega)^2}}. \tag{15}$$

Here ω_c is the central frequency of the emitted field and $\Delta\omega$ is its Full Width at Half Maximum.

Naturally, both the central frequency and the bandwidth depend on the geometry:

$$\omega_c(\theta,\delta) = 2\frac{[a^2 - a(1+b) + 1 + b]}{2 + 2a^2 + 4b + 3b^2 - 2a(1+2b)}\omega_0$$
$$\Delta\omega_s(\theta,\delta) = 2\sigma\sqrt{\log 2}\sqrt{\frac{2(1+a+a^2)}{(2+2a^2+4b+3b^2) - a(2+4b)}} \quad (16)$$

where the coefficients a and b are given by Eq. (13). The second square root in the expression for $\Delta\omega_s$ provides a "narrowing factor", defining the ratio between the bandwidth of the incident pulse and the bandwidth of the generated FWM.

For square boxcars configuration $\delta = 0$, we obtain: $\omega_c(\theta,0) = \omega_0$ and $\Delta\omega_s(\theta,0) = 2\sigma\sqrt{\log(2)}/\sqrt{3}$. As could be expected for this symmetric configuration, the central frequency of the emitted signal coincides with the carrier frequency of the laser, but the bandwidth is narrower than that of the laser pulse by a factor of $\sqrt{3}$, and thus by a factor of 3 narrower than that of the signal generated by focused beams (see Eq. (8) above).

For small deviations of the Stokes beam from the square boxcars geometry ($\delta \ll \theta$), Eq. (16) reduces to

$$\omega_c(\theta,\delta) \simeq \omega_0\left(1 - \frac{4}{3}\delta\cot\theta\right), \quad (17)$$

Eq. (15) shows that for small deviations, the detuning of the Phase Matching Filter from the laser frequency is linear with the angular deviation of the Stokes beam. This derived analytical result is plotted as a solid line in Fig. 2b. The simple dependence provides a convenient means for spectral scanning of the frequency of the phase-matched FWM signal.

So far, the derivation was performed for well collimated beams. However, divergence of the beams will modify the experimental results. For simplicity, we calculate the effect of the divergence of the Stokes beam (the one that is being changed) on the bandwidth of the phase matching filter. The divergence of the other beams may be included in a similar manner.

The spectral intensity of the generated signal is given by

$$\langle I(\omega_s,\theta)\rangle = |\frac{1}{2\alpha_{div}}\int_{-\alpha_{div}}^{\alpha_{div}} E_{PM}(\omega_s;\theta,\delta)d\delta|^2.$$

Here $\langle I(\omega_s,\theta)\rangle$ is the intensity of the signal at frequency ω_s integrated over the divergence angle α_{div}, and $E_{PM}(\omega_s;\theta,\delta)$ is given by Eq. (14). In other words, we average over all directions within the divergence angle. The calculation was performed numerically for a range of divergence angles. Fig. 3 depicts the ratio of the calculated bandwidth to the bandwidth of the theoretically derived limit for perfectly collimated beams (Eq. (15)). For our experimental conditions, 4 mrad diverging (converging) beams will exploit the entire available bandwidth, which is equivalent to the fully focused case ($3\Delta\omega_{col}$), as would result from Eq. (8). The experimentally used divergence was much smaller.

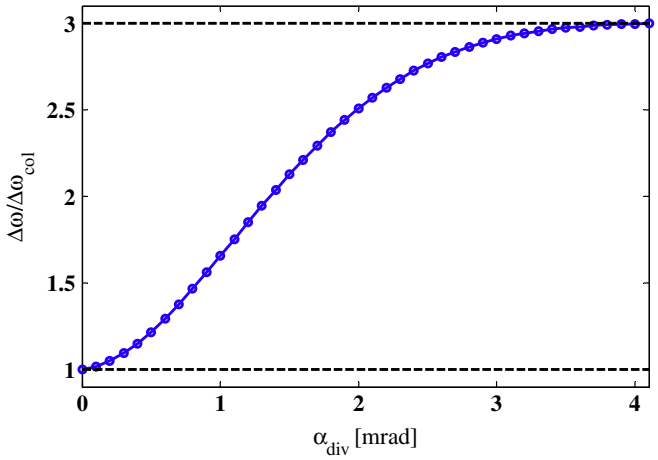

Fig. 3. Numerically calculated bandwidth (in units of FWHM of collimated case) of a signal for various of beams' divergence angles.

5. Measurements with the combined PMF and single shot methods

In what follows we combine the PMF with the single shot method for measuring spectrally AND temporally resolved FWM in chloroform. The experimental conditions are as follows: the cross section of the collimated incident beams is 7 mm, the angle between pump and probe beams is 140 mrad (~8°), and the beam divergence angle was measured to be 0.3 mrad. Neat spectroscopic grade chloroform was used as purchased from Sigma–Aldrich. The sample was placed in a 25 mm long spectroscopic cell. The laser pulses are derived from Spectra-Physics Oscillator (Tsunami) and amplified in a Spectra-Physics Chirped pulse amplifier (Spitfire). The pulses are 60 fs long, centered at 800 nm, and the total energy at the entrance to the cell is ~0.5 mJ. The FWM beam is imaged on an ISG-1394-S CMOS camera.

To ensure that every image is indeed produced by single laser pulse, the repetition rate of the laser was reduced to 10 Hz, and the exposure of the camera is set to 40 ms. The angular tuning of the Stokes beam is achieved by fine angular rotation of the last folding mirror before the cell, and is measured as a displacement of this beam on a target located several meters away. The spectral calibration of each set of experiments is performed by measuring the spectrum of the coherence spike (signal generated at the coincidence of all three pulses) with JY TRIAX 180 monochromator coupled to the CCD camera.

The spectral narrowing was measured to be ~8% smaller than what would be expected for collimated beams, which is compatible with the measured divergence angle of 0.3 mrad (Fig. 3).

To ascertain that the beam divergence, due to diffraction or self focusing, was insignificant, we observed the actual beam divergence upon exit from the cell on a screen 10 m away, and also compared the spectral width of the beams before and after the cell. Both the spatial and spectral properties of the beams were unaffected by their propagation through the cell.

By tuning the angle δ we obtain a series of time resolved images, each measured within a single laser shot. An example of such an image is shown in (Fig. 4a) for the angle $\delta = 0, \Delta_c = 0$, the retrieved temporal profile is shown at the inset of the panel. Measurements like the one depicted in Fig. 4a are repeated for a range of angles, each such temporal profile is Fourier Transformed, to produce a line in the two-dimensional map (Fig. 4b) of the power spectrum (vertical axis) of the FWM signal (in the Supplementary Material we provide a series of data collected from 40 measurements taken at different angles δ, shown as a movie for the signal dependence on the angle of the stokes pulse. Each picture in the movie is used to extract the time resolved profile such as the inset to Fig. 4a, which in turn is Fourier transformed to give a line in the two-dimensional map).

The data included in Figs. 1b and 4b are in principle equivalent; the spectral and temporal resolutions are parameters of choice, determined by the spectrometer resolution on the one hand, and the number of measured angles on the other. The experimental simplicity of the Single-Shot PMF measuring method offers significant advantages: once calibrated, a spectrometer is not used and critical alignment is not required to conduct the measurement, the experiment involves broad unfocused beams crossing in the sample. Moreover, since there are no mechanical scans of time

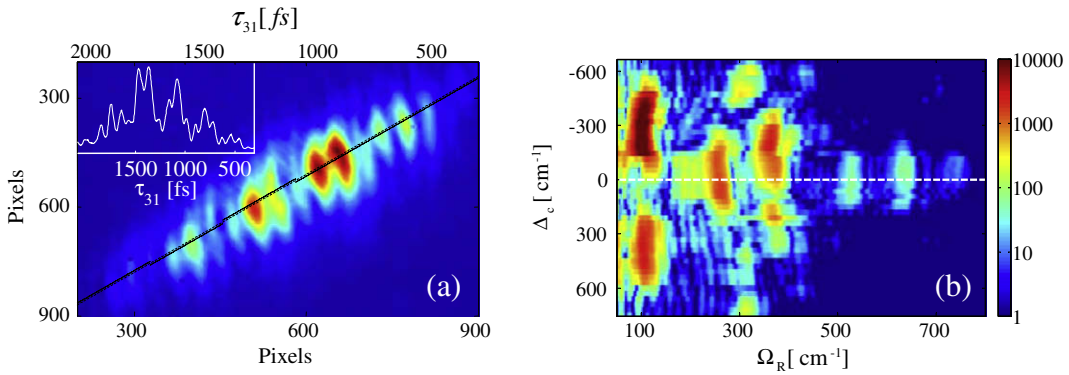

Fig. 4. (a) Typical Single Shot FWM image of chloroform with the TRFWM signal in the inset. (b) Two-dimensional spectrogram of the chloroform Raman FWM signal obtained by phase matching filtering, where the power spectrum of the FWM signal is plotted horizontally against the Raman frequency (Ω_R) and vertically against (Δ_c), the detuning of the PMF from the laser center frequency (The intensity is plotted on a log scale).

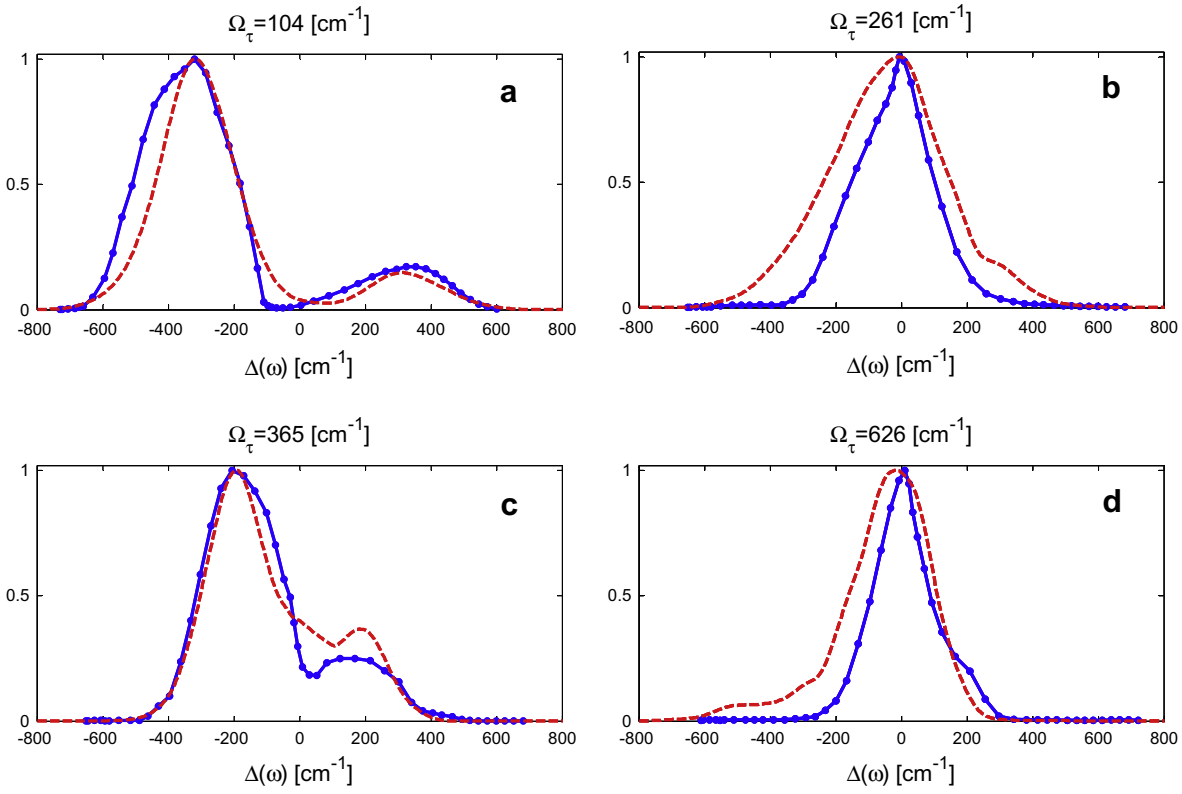

Fig. 5. Detuning dependence (normalized) of the Raman contributions and a comparison between the 2D-spectrograms obtained by the Spectrally Resolved Temporal Scanning method (red dashed lines) and by the Single-Shot PMF method (blue lines with solid circles). (a) Depicts section of both spectrograms along $\Omega_R = 104cm^{-1}$, (b) along the $\Omega_R = 261cm^{-1}$, (c) $\Omega_R = 365cm^{-1}$ and (d) $\Omega_R = 626cm^{-1}$. (For interpretation of the references to color in this figure legend, the reader is referred to the web version of this article.)

Table 2
The fundamental vibrational frequencies of chloroform.

Vibration	Character	Energy(cm^{-1})
ν_1	C-H *s* stretch	3021
ν_2	CCl_3 *s* stretch	680
ν_3	CCl_3 *s* deform	365
ν_4	C-H *d* bend	1220
ν_5	CCl_3 *d* stretch	774
ν_6	CCl_3 *d* deform	261

delays, and since the entire measurement may be derived within a single ultrafast pulse per spectral point, a full measurement may be performed with very few laser pulses – a crucial requirement for molecules undergoing rapid photobleaching as is the case for many molecules of biological interest [22].

Consider the spectrogram shown in Fig. 4b:

There are several distinct spectral features at: 104, 261, 300, 365, 520, 625 and 730 cm^{-1}. The bandwidth of our pulses does not allow the observations of features at higher frequencies. Fig. 5 depicts, for several of these features, vertical cuts in Figs. 1b and 4b, showing the intensity distribution at a given Raman frequency Ω_R as a function of the detuning Δ_c from the laser center frequency. In Fig. 5, the spectral profiles are given for both measurement methods, those obtained by acquiring a full

spectrum at a given delay (Fig. 1b), and by the newly introduced method of Single-Shot PMF (Fig. 4b).

The known fundamental mode frequencies of chloroform are given in Table 2.

The results obtained by both methods are similar, and will be discussed together. The spectral profile for both $\Omega_\tau = 104\,\mathrm{cm}^{-1}$ and $\Omega_\tau = 365\,\mathrm{cm}^{-1}$ show double maxima, peaking at $\Delta(\omega) = \pm 310\,\mathrm{cm}^{-1}[\simeq (261+365)/2]$ and $\Delta(\omega) = \pm 183\,\mathrm{cm}^{-1}$ $[\simeq 365/2]$, respectively. The spectral profile of the $\Omega_\tau = 261\,\mathrm{cm}^{-1}$ line should have shown a double maximum at $\Delta(\omega) = \pm 130\,\mathrm{cm}^{-1}[\simeq 261/2]$, but these are unresolved due to the convolution with the $400\,\mathrm{cm}^{-1}$ pulse. The peaks at $522\,\mathrm{cm}^{-1}$ (=261×2), $730\,\mathrm{cm}^{-1}$ (=365×2) and $626\,\mathrm{cm}^{-1}$ (=261 + 365) are centered at $\Delta(\omega) = 0$ as theoretically predicted for interference between contributions of two spectroscopic pathways. The fact that the double peak lines are asymmetric in their intensity is not yet fully understood and requires further study.

6. Conclusions

In conclusion, we have discussed in detail the advantages offered by the combined Time-Frequency Domain FWM. We demonstrated that while the basic spectral information (i.e. the measured frequencies) may be derived from simple time resolved measurements, the combined TFD measurements characterize the individual lines and identifies them as either fundamental modes or beat frequencies between such modes. We further showed that in time resolved FWM spectral data is essential to attribute particular lines to the proper Feynman diagram, as well as for identification of the beat frequencies stemming from the interferences of various spectroscopic pathways. We have introduced and demonstrated a new approach to TRFWM, where the entire time domain signal is captured within a single pulse. By taking advantage of the unique geometrical arrangement, we use Phase Matching Filtering, where the collimated beams impose well defined phase matching conditions on the intersecting beams, such that only a narrow-frequency section of the spectrally broad pulses is being phase matched, and therefore it is only this relatively narrow frequency range that contributes to the FWM signal. We demonstrated the method experimentally, and performed detailed comparison to data obtained by the traditional approach. The Single-Shot PMF method offers significant advantages, being fast and efficient in terms of the number of laser pulses used for the entire measurement, and experimentally simple. Because of its inherent speed, the new method has a promising potential for the characterization of short lived optically unstable molecules.

Experiments are under way with more complex molecules, and for the implementation of the method for studying transient excited electronic states.

Acknowledgements

We gratefully acknowledge discussions with Ilya Averbukh, Sharly Fleischer and Mark Vilensky. This work was supported by the Nancy and Steve Grand Center for Sensors and Security, by a James Franck Minerva grant, and by the Israel Science Foundation.

References

[1] D.M. Jonas, Annu. Rev. Phys. Chem. 54 (2003) 425.
[2] D. Keusters, H.S. Tan, W.S. Warren, J. Phys. Chem. A 103 (1999) 10369.
[3] M.H. Levit, Spin Dynamics, John Willey and Sons, Ltd., Chichester, 2001.
[4] S. Mukamel, Principles of Nonlinear Optical Spectroscopy, Oxford University Press, New York, 1995.
[5] M. Heid, S. Schlucker, U. Schmitt, T. Chen, R. Schweitzer-Stenner, V. Engel, W. Kiefer, J. Raman Spectrosc. 32 (2001) 771.
[6] B.D. Prince, A. Chakraborty, B.M. Prince, H.U. Stauffer, J. Chem. Phys. 125 (2006) 044502.
[7] S. Nath, D.C. Urbanek, S.J. Kern, M.A. Berg, Phys. Rev. Lett. 97 (2006) 267401.
[8] S. Nath, D.C. Urbanek, S.J. Kern, M.A. Berg, J. Chem. Phys. 127 (2007) 044307.
[9] S.O. Konorov, X.G. Xu, R.F.B. Turner, M.W. Blades, J.W. Hepburn, V. Milner, Opt. Express 15 (2007) 7564.
[10] X.J.G. Xu, S.O. Konorov, S. Zhdanovich, J.W. Hepburn, V. Milner, J. Chem. Phys. 126 (2007) 091102.
[11] R. Trebino, Frequency-Resolved Optical Gating: The Measurement of Ultrashort Laser Pulses, Kluwer Academic Publishers, Boston, 2002.
[12] Y. Paskover, I.S. Averbukh, Y. Prior, Opt. Express 15 (2007) 1700.
[13] Y. Prior, Appl. Opt. 19 (1980) 1741.
[14] D.C. Urbanek, M.A. Berg, J. Chem. Phys. 127 (2007) 044307.
[15] Y. Prior, IEEE J. Quant. Electron. 20 (1984) 37.
[16] A. Shalit, Y. Paskover, Y. Prior, Chem. Phys. Lett. 450 (2008) 408.
[17] J.A. Shirley, R.J. Hall, A.C. Eckbreth, Opt. Lett. 5 (1980) 380.
[18] P. O'Shea, M. Kimmel, X. Gu, R. Trebino, Opt. Lett. 26 (2001) 932.
[19] D. Romanov, A. Filin, R. Compton, R. Levis, Opt. Lett. 32 (2007) 3161.
[20] N. Belabas, D.M. Jonas, J. Opt. Soc. Am. B 22 (2005) 655.
[21] A.N. Naumov, A.M. Zheltikov, J. Raman Spectrosc. 32 (2001) 960.
[22] H. Kawano, Y. Nabekawa, A. Suda, Y. Oishi, H. Mizuno, A. Miyawaki, K. Midorikawa, Biochem. Biophys. Res. Commun. 311 (2003) 592.